S7-05

156194

13P

**N88-27155**

# A COMPARISON OF THEORY AND FLIGHT TEST OF THE BO 105/BMR IN HOVER AND FORWARD FLIGHT

Paul H. Mirick
Aerospace Engineer
U.S. Army Aerostructures Directorate
Hampton, Virginia

## Abstract

Four cases were selected for comparison with theoretical predictions using stability data obtained during the flight test of the Bearingless Main Rotor (BMR) on a Messerschmidt-Boelkow-Blohm BO 105 helicopter. The four cases selected from the flight test include two ground resonance cases and two air resonance cases. The BMR used four modified BO 105 blades attached to a bearingless hub. The hub consisted of dual fiberglass C-channel beams attached to the hub center at 0.0238R and attached to the blade root at 0.25R with blade pitch control provided by a torque tube. Analyses from Bell Helicopter Textron, Boeing Vertol, and Sikorsky Aircraft were compared with the data and the correlation ranged from very poor-to-poor to poor-to-fair.

## Introduction

As part of the Methodology Assessment, four cases were selected from the flight test reported in Ref. 1 for a comparison with theoretical predictions. The test reported in Ref. 1 was conducted by the Boeing Vertol Company as part of the U.S. Army Applied Technology Laboratory program to design, fabricate, and demonstrate by flight test, the feasibility of the Bearingless Main Rotor (BMR). The flight testing included investigation of ground resonance characteristics on both concrete and turf surfaces as well as air resonance characteristics in hover, forward flight, rearward flight, sideward flight, and climbs and descents. From the extensive stability data obtained during the BMR flight test program, two ground resonance and two air resonance cases were selected for comparison with theoretical predictions. The two ground resonance cases were selected with different landing gear configurations as this affected the body frequency and, hence, the aeromechanical stability. One air resonance case was selected with airspeed as the independent variable, and the second was selected with climb rate (inflow) as the independent variable.

The theoretical models compared with the data included the Bell Helicopter DRAV21 and C81 analyses, the Boeing Vertol C-90 code, and the Sikorsky E927-3 analysis for the hover cases. Neither Hughes Helicopters nor the U.S. Army Aeromechanics Laboratory modeled these cases.

This paper briefly describes the tests from which the data were obtained and presents the correlation. Conclusions as to the quality of the agreement between theory and test are presented. Appendices are provided that document the test aircraft and rotor system properties, tabulate the experimental data points, and show all of the correlations.

## Flight-Test Program

A Messerschmidt-Boelkow-Blohm BO 105 helicopter flight-test program with a Bearingless Main Rotor (BMR) installed was conducted by Boeing Vertol as part of the U.S. Army Applied Technology Laboratory program to design, fabricate, and demonstrate by flight test the feasibility of the BMR.[1] Testing included the determination of ground resonance characteristics on both concrete and turf landing surfaces, as well as the determination of air resonance characteristics in hover, forward flight, rearward flight, sideward flight, climb, and descent. Flight loads, flying qualities, and vibration surveys were also conducted as part of this test. The results from this test provided a data base for the methodology assessment, which allowed a comparison of computer code predictions with actual flight test data.

## Test Vehicle Description

The BMR installed on the BO 105 is shown in Fig. 1. The blades are modified BO 105 blades attached to a set of dual fiberglass beams at 0.25R with the beam roots attached at 0.0238R to a metal hub-plate set. All the geometric parameters of the

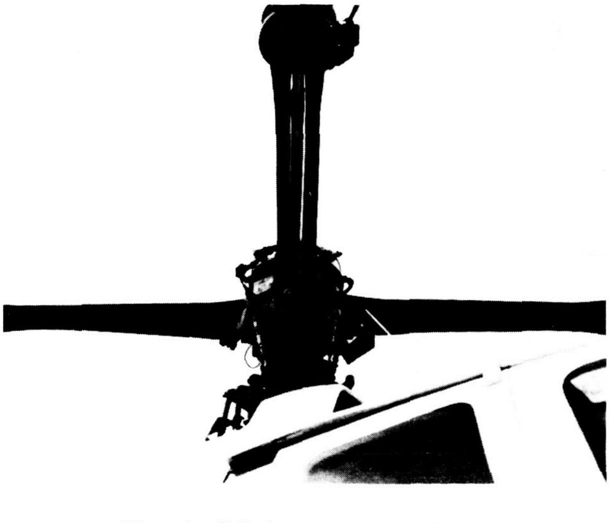

Fig. 1 BMR installed on BO 105.

individual beams, such as width, height, flange and web thickness, and spacing between the beams, vary along the length. The fiberglass beams permit flapwise bending, chordwise bending, and full torsional travel. The flap, chord, and torsional frequencies of the rotor were designed to be approximately the same as those of the BO 105 rotor system. Blade pitch is controlled by a filament-wound graphite torque tube. The outboard end of the torque tube is cantilevered at the blade-to-beam joint and supported at its inboard end by a rod end bearing. The fiberglass beams have a C-channel cross section. Detailed rotor characteristics are given in Appendix A.

The BMR hub was attached to the rotor shaft of the BO 105 helicopter through the same hole pattern as the standard hub. Because of the difference in the pitch arm attachment locations, new pitch links were fabricated. Initial ground resonance testing showed an unacceptable level of damping and, as a result, the landing gear was modified by adding two cables stretched between the left- and right-side skids as shown in Fig. 2. This resulted in an increase in the aircraft pitch and longitudinal mode frequencies and raised the critical rotor speed for ground resonance.

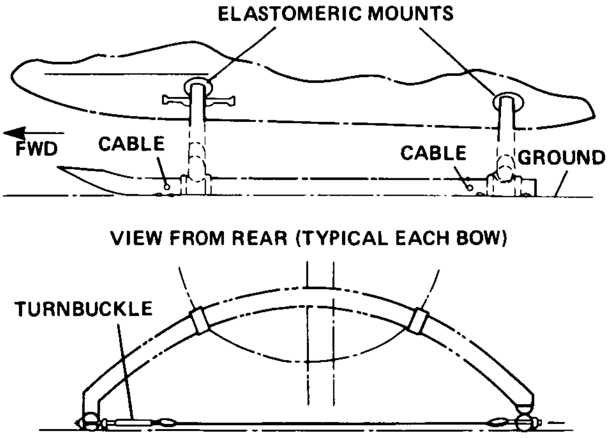

Fig. 2 Stiffening modification for BO 105 landing gear.

## Test Procedure

To obtain ground or air resonance data, the aircraft was trimmed at the desired test condition. The pilot would then excite the air or ground resonance mode by moving the cyclic stick in a whirling motion at a predetermined frequency using 5% of total stick amplitude. After about eight cycles, the excitation was stopped and the blade chordwise modal decay was analyzed to determine the damping characteristics.

Two methods were used to determine air or ground resonance damping from the test data. The first method obtained the damping from the logarithmic decrement of the decay envelope as faired by hand. The second method used a computerized moving-block method to determine damping. Results obtained using both methods are contained in Ref. 1.

## Test Results

Detailed results for the BMR flight tests are contained in Volumes 1 and 2 of Ref. 1 and a summary of results is contained in Ref. 2. Ground resonance data were obtained for the aircraft on concrete commencing at 75% $N_R$ with flat pitch and incrementally building up to and including 95% $N_R$. Takeoffs were made at 95% $N_R$ and landings were made on a concrete surface at rotor speeds of 95, 97.5, 100, and 102% $N_R$. Trimmed conditions were established at several settings between touchdown collective pitch and flat pitch. Pilot cyclic stick excitation was introduced at the appropriate frequency at each of these collective pitch settings and damping was computed from the decay of the chord bending after cyclic pitch excitation was stopped. Damping results were stable for 95, 97.5, and 100% $N_R$ for touchdown collective pitch to flat pitch. Damping generally decreased with collective pitch, but showed a dip at a collective pitch between the touchdown and flat pitch values. This dip was different for each rotor speed. At 102% $N_R$, the trend below 25% collective pitch indicated a possible instability at about 15%; therefore, the test was cut off at 17% collective pitch. A possible degradation of the ground resonance mode damping was anticipated for landings on a turf surface because of the expected reduction of the body longitudinal-pitch frequency. Testing on turf was performed at 95% $N_R$. The damping trend indicated a possible instability at a collective pitch of about 22% and, therefore, the test was stopped at 28% $N_R$. To avoid this potential instability, the landing gear was stiffened by installing a wire cable between the skids (as has been shown in Fig. 2), and the ground resonance testing was repeated. Later analysis and aircraft shake testing showed that the predominant mode at the critical frequency on the ground had more longitudinal motion than pitch motion. A comparison of damping obtained for the 102% $N_R$ case on concrete is shown in Fig. 3. Tests were then conducted on a turf surface once an acceptable damping level was demonstrated on a concrete surface.

Forward-flight testing was performed out to $V_H$ of 109 knots for level flight and 135 knots in a maximum power descent once adequate rotor stability was demonstrated in hover and on the ground. Forward flight stability testing also included aircraft climbs/descents and autorotations.

## Selection of Test Cases

Two ground resonance and two air resonance cases were selected for comparison with predictions. The first ground resonance case selected,

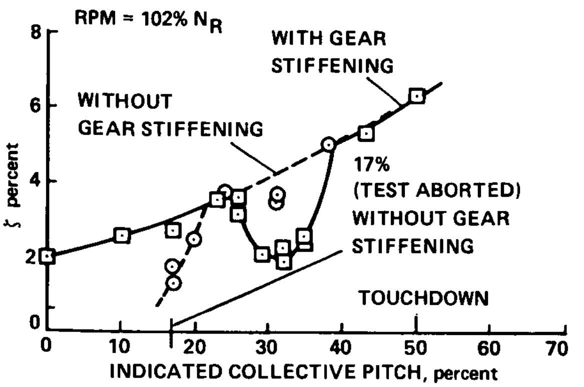

Fig. 3 BMR ground-resonance damping on concrete.

Case 1, was the BO 105/BMR on concrete, with standard gear and rotor operating at 102% of normal rotor speed. This case was selected because of the reduced stability at low collective pitch angle. The other ground resonance case selected, Case 2, was for the same conditions, but with the stiffened landing gear. The first air resonance condition selected, Case 3, was for the airspeeds from hover to 109 knots. This provided an assessment of the predictions over the full range of airspeeds. Case 4 examined the aeromechanical stability at an airspeed of 50 knots for a collective range of 0 to 6%. This case included the lowest damping that was encountered in forward flight.

## Correlation

The ground resonance cases in hover were modeled by Bell Helicopter Textron with the DRAV21 analysis; Boeing Vertol used the C-90 analysis and Sikorsky used the E927-3 code. For the forward-flight air resonance cases Bell Helicopter Textron used C81 and Boeing Vertol used C-90 again. Sikorsky did not model the forward flight cases.

The comparison of the predicted and measured regressing lead-lag mode damping as a function of collective pitch is shown in Figs. 4 and 5 for the ground resonance cases. One difficult aspect of predicting ground resonance is that the aircraft body frequencies vary as the rotor thrust increases and the aircraft lifts off the ground. Bell Helicopter Textron estimated the variation of body pitch frequency with collective pitch from the known frequencies at flat pitch on the ground (3.08 Hz) and in hover (1.0 Hz). They assumed that at 7% indicated collective pitch that the body pitch frequency crossed over the lead-lag regressing mode. A curve for body frequency as a function of indicated collective pitch was generated using these values. For the cases with the stiffened landing gear, a body frequency of 3.28 Hz was used at flat pitch; 1.0 Hz for hover; and the coalescence was assumed at 32% indicated collective. A comparison of the DRAV21 results with the test data for the two ground resonance cases (Figs. 4 and 5)

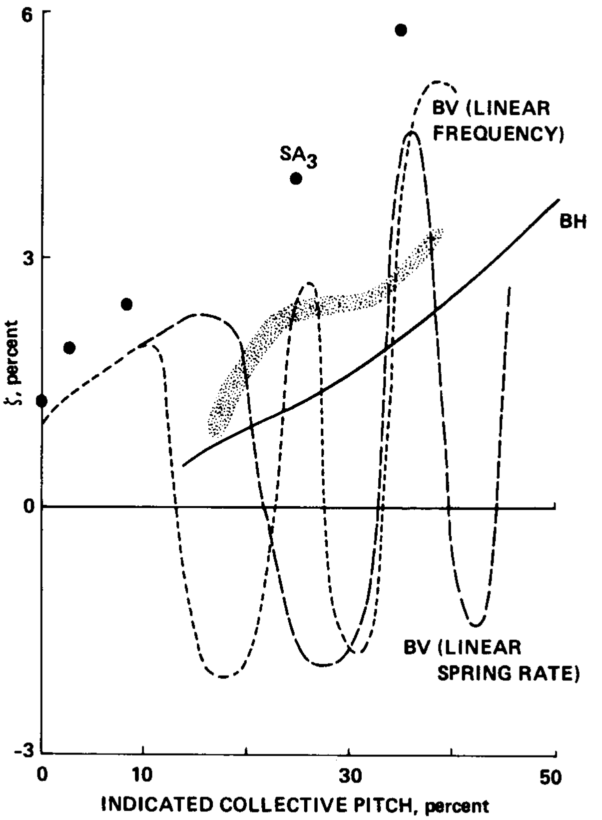

Fig. 4 Regressing lead-lag mode damping as a function of collective pitch; 102% $N_R$, standard gear, concrete surface.

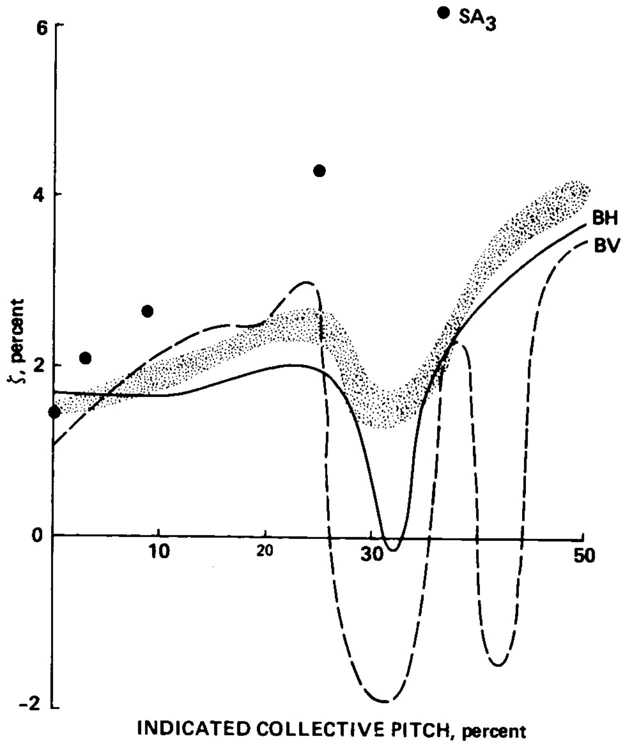

Fig. 5 Regressing lead-lag mode damping as a function of collective pitch; 102% $N_R$, stiffened gear, concrete surface.

shows that the analytical results follow the trend of the test data, but underpredict the level of damping. The correlation for both of these cases was judged to be poor-to-fair.

Boeing Vertol assumed that for the standard gear that either the landing-gear spring rate or the body mode frequency varied linearly with thrust; both predictions are shown in Fig. 4. For the stiffened gear, Boeing used only the linear spring rate. Both the linear frequency and the linear spring rate assumptions show two areas of instability for Case 1: a roll-lateral mode and a pitch-longitudinal mode. The first unstable region, the pitch-longitudinal mode, occurs at approximately the same collective setting at which the test data showed a large decrease in damping. The correlation for both cases is considered very poor-to-poor.

Sikorsky modeled the two ground resonance cases using the E927-3 analysis. The analysis overpredicts the damping level for all collective pitch angles except 0° in the stiffened gear case. No effect of a change in body mode frequency is observed in these predictions as the collective pitch is changed. The correlation is judged to be very poor-to-poor for both cases.

The two air resonance cases were modeled by Bell Helicopter Textron and Boeing Vertol. The data and the predictions for the two cases are compared in Figs. 6 and 7. The first air resonance case, Case 3, shows the regressing lead-lag mode damping as a function of airspeed. The C81 analysis shows a minimum in the damping at about 70 knots which is higher than the 40-knot minimum that is seen in the data. The damping level is considerably underpredicted so overall the correlation is considered to be poor-to-fair. The Boeing Vertol C-90 prediction shows the minimum in the damping at about 60 knots which is, again, higher than the minimum indicated by the data. The damping level prediction is better than seen for the C81 analysis so overall the correlation is judged fair.

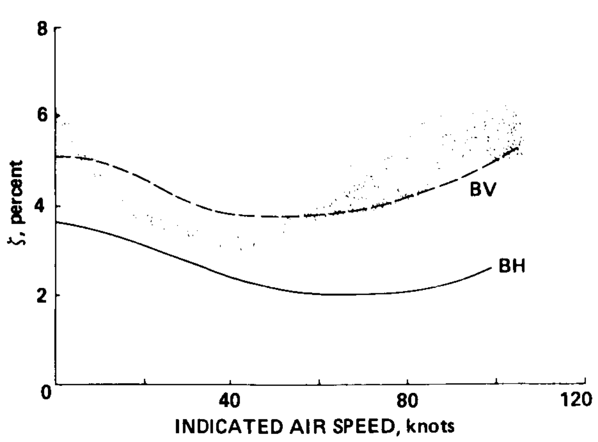

Fig. 6 Regressing lead-lag mode damping as a func- of airspeed.

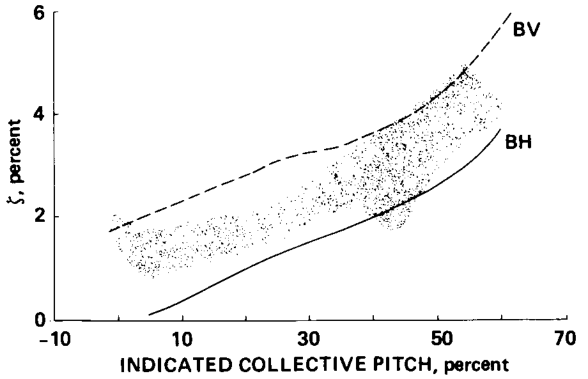

Fig. 7 Regressing lead-lag mode damping as a function of collective pitch at 50 knots.

The second air resonance case, Case 4, shown in Fig. 7, plots the regressing lead-lag mode damping as a function of indicated collective pitch as the aircraft is flown at climb and descent trimpoints at 50 knots. The Bell Helicopter Textron C81 analysis shows the trend with collective pitch correctly, but the damping level is underpredicted. The correlation is judged to be poor-to-fair. The Boeing Vertol C-90 code also predicts the correct trend with collective pitch, but overpredicts the level of damping. The correlation is considered fair.

## Conclusions

Four analyses were compared with one or more cases from a flight test of the BMR on a BO 105 helicopter that measured the lead-lag regressing mode frequency and damping. The four cases selected from the flight test included two ground-resonance cases and two air-resonance cases. Based on a comparison of the analyses and the experimental data, the following conclusions were reached.

1. The DRAV21 analysis used by Bell Helicopter Textron for the ground resonance cases gave poor-to-fair correlation. The C81 analysis used for the air resonance cases also gave poor-to-fair correlation.

2. The C-90 analysis used by Boeing Vertol gave very poor-to-poor correlation for the ground resonance cases and fair correlation for the air resonance cases.

3. The E927-3 analysis used by Sikorsky for the two ground resonance cases gave very poor-to-poor correlation.

## References

[1] Staley, James A. and Reed, Donald A., "Aeroelastic Stability and Vibration Characteristics of a Bearingless Main Rotor," Boeing Vertol Company Report D210-11498-1, June 1979.

[2] Dixon, Peter G. C., "Design Development, and Flight Demonstration of the Loads and Stability Characteristics of a Bearingless Main Rotor," USAAVRADCOM TR-80-D-3, June 1980.

## Appendix A - Test Aircraft Properties

The four cases examined in this paper are from a flight test program originally reported in Refs. 1 and 2. The experimental properties in this appendix are taken from those references.

### Rotor Description

The Bearingless Main Rotor (BMR) system is compatible in physical, dynamic and static characteristics to the current BO 105 rotor system. The BMR has no pitch bearing and no flapping or lead-lag hinges; it uses a flexible hub construction to accommodate control-system pitch inputs and normal flapping motion. The BMR assembly is shown in Fig. 8.

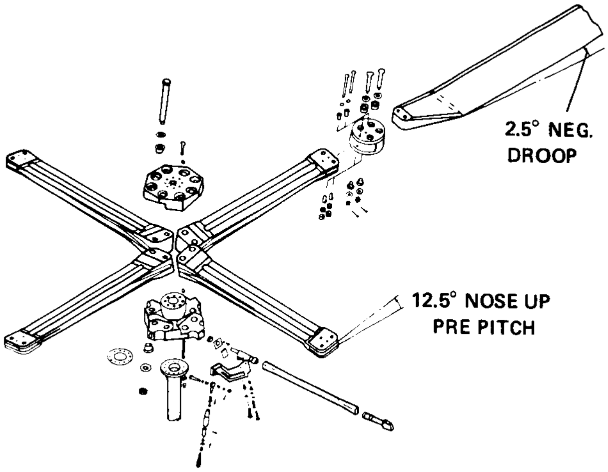

Fig. 8 BMR blade and hub arrangement.

The rotor blades used for the BMR are essentially standard BO 105 main rotor blades from the 70-in. blade station to the tip (blade station 193.37 in.). The inboard end was redesigned to replace the conventional swan-neck and single-pin wraparound retention with a double-pin wrap concept on the blade at a blade station of 52.36 in. The blades are attached to the beam flexure through a titanium clevis such that the beam is untwisted when the blade chord line at 0.70R is at a pitch angle of 9.55°. The flexbeam chord axis is at a pitch angle of 12.5° with respect to the hub. The outboard two-pin attachment of the beam to the clevis is at blade station 4.6 in. To improve the aeroelastic stability characteristics, the blade is preconed by 2.5° at the beam-to-blade clevis. The rotor blade has a constant NACA 23012 airfoil distribution and a 10.63-in. chord. The geometric twist for the blade and a comparison of the BMR blade planform with the BO 105 blade are given in Fig. 9. The spanwise mass moment can be fine-tuned with the changeable-tip weight system. The second flap and chord frequencies can be fine-tuned by adding weight to a cavity in the blade at approximately the 50% radial station. Up to four pounds of tungsten can be accommodated. Leading edge erosion protection is retained by including the standard BO 105 titanium leading-edge segments. The blade and clevis properties are summarized in Table 1.

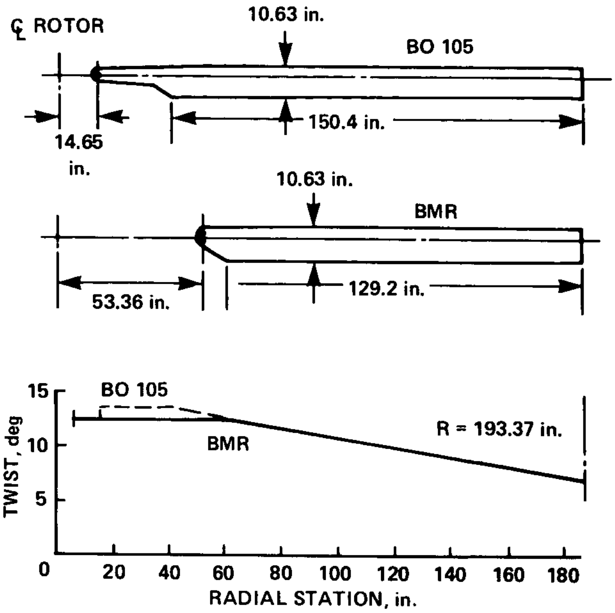

Fig. 9 BMR and BO 105 rotor blade planform and geometric twist.

Blade pitch-control motion is transmitted from the standard pitch link through a pitch arm attached to a filament-wound graphite torque tube. The torque tube is rigidly attached to the blade clevis at the outboard end and supported in a spherical bearing inboard.

The fiberglass beams which accommodate the flapping and lead-lag motion have a C-channel cross section, with the geometric parameters of spacing between the beams varying over the length of the beam. Data for the beams are given in Table 2. The two beams are separated by a gap to provide space for the pitch-control torque tube and are joined at the inboard and outboard ends by steel-plate shear ties. A loop at both the inboard and outboard upper and lower flange ends provides a continuous fiber load-path to retain the attached blade against centrifugal force, flap and chordwise loads. Steel bushings inside each loop provide a shear tie reinforcement between the upper and lower flanges and protect the attachment pins from the fibrous composite material. Stress concentrations in the inboard fiber wrap are relieved by an additional web-wrap reinforcement between the upper and lower flanges. The internal and external crossply wraps provide a shear connection between the upper and lower flanges together with the required shear reinforcement to the unidirectional material. A steel hub plate accommodates the beam-to-shaft attachment and provides a prepitch angle of 12.5°. The flap-lag coupling which results from this feature improves the aeroelastic stability characteristics of the rotor system.

## Aircraft Characteristics

The test aircraft used was a standard Messerschmidt-Boelkow-Blohm BO 105 helicopter with some minor modifications. Because the torisonal rigidity of the BMR beam flexures was greater than the BO 105 (141 in.-lb/deg versus 45 in.-lb/deg), the control loads were expected to be higher. In order to offset these higher control loads and provide a greater control margin, it was necessary to increase the hydraulic boost pressure from 1500 to 2000 psi. Another modification required was to fabricate shorter pitch links to accommodate the difference in the pitch arm attachment location of the BMR and the standard BO 105 rotor. A third modification was made to the aircraft when the preliminary ground resonance flight tests showed the need for stiffening the landing gear in order to increase the critical rotor speed for ground resonance.

The BO 105 properties needed to model the aircraft in the Boeing Vertol C-45 math model are summarized in Table 3. The C-45 model was used to compute the air and ground resonance characteristics for the BO 105. The sources of this data include test results, physical measurements, and computed results. A representation of the C-45 model is shown in Fig. 10. It should be realized that in determining the fuselage inertias, the C-45 model breaks the fuselage inertia into three components: fuselage, pylon, and tail. Each individual inertia is defined about its own c.g. so a calculation of complete inertia requires the appropriate transformation and summation of inertia. The rotor mass is not included in these computations.

Table 1 Blade and Clevis Properties

| R, in. | r/R | Wt/in., lb/in. | EI-Flap, $EI_f$, $10^6$ lb/in.$^2$ | EI-Chord, $EI_c$, $10^6$ lb/in.$^2$ | Torsional Stiffness, GK, $10^6$ lb/in.$^2$ |
|---|---|---|---|---|---|
| 193.37 | 1.0 | 0.71 | 2.38 | 59.4 | 1.36 |
| 192.02 | 0.993 | 0.71 | 2.38 | 59.4 | 1.36 |
| 192.02 | 0.993 | 0.511 | 2.38 | 59.4 | 1.36 |
| 188.92 | 0.997 | 0.511 | 2.38 | 59.4 | 1.36 |
| 186.99 | 0.967 | 0.32 | 2.38 | 59.4 | 1.36 |
| 153.92 | 0.796 | 0.32 | 2.38 | 59.4 | 1.36 |
| 153.92 | 0.796 | 0.309 | 2.38 | 59.4 | 1.36 |
| 97.65 | 0.505 | 0.309 | 2.38 | 59.4 | 1.36 |
| 97.65 | 0.505 | 1.447 | 2.38 | 59.4 | 1.36 |
| 95.72 | 0.495 | 1.447 | 2.38 | 59.4 | 1.36 |
| 95.72 | 0.495 | 0.309 | 2.38 | 59.4 | 1.36 |
| 87.79 | 0.454 | 0.309 | 2.38 | 59.4 | 1.36 |
| 81.99 | 0.424 | 0.309 | 2.38 | 59.4 | 1.55 |
| 76.19 | 0.394 | 0.372 | 3.39 | 56.71 | 1.74 |
| 66.52 | 0.344 | 0.4762 | 5.084 | 52.21 | 3.02 |
| 62.85 | 0.325 | 0.5159 | 5.725 | 50.51 | 3.80 |
| 59.94 | 0.304 | 0.5474 | 6.234 | 49.16 | 4.07 |
| 53.95 | 0.279 | 0.6121 | 7.281 | 46.375 | 4.10 |
| 53.95 | 0.279 | 2.573 | 82.28 | 68.375 | 5.10 |
| 52.0 | 0.269 | 2.573 | 157.28 | 266.375 | 5.77 |
| 50.4 | 0.2607 | 2.573 | 164.4 | 291.38 | 6.32 |
| 50.4 | 0.2607 | 1.3725 | 164.4 | 521.38 | 41.13 |
| 49.75 | 0.2573 | 1.359 | 167.28 | 566.95 | 41.13 |

Table 2 Physical Properties of Dual Flexbeam

| R, in. | Width W, in. | Height H, in. | $t_{Flange}$ $t_f$, in. | $t_{Web}$ $t_w$, in. | $EI_f$, $10^6$ lb/in.$^2$ | $I_f$, $lb_m \cdot in.^2$ | $EI_c$, $10^6$ lb/in.$^2$ | $I_c$, $lb_m \cdot in.^2$ |
|---|---|---|---|---|---|---|---|---|
| 4.6 | 2.875 | 3.526 | 1.201 | 1.250 | 58.1600 | 15.992 | 380.8900 | 44.351 |
| 5.3 | 2.770 | 3.526 | 1.156 | 2.718 | 98.8550 | 20.223 | 392.3630 | 74.521 |
| 6.3 | 2.600 | 3.526 | 1.092 | 2.336 | 92.0356 | 18.593 | 350.1850 | 63.489 |
| 8.3 | 2.280 | 3.055 | 0.895 | 1.651 | 60.0551 | 10.617 | 235.5785 | 40.144 |
| 10.3 | 1.960 | 2.583 | 0.699 | 1.056 | 30.9167 | 5.379 | 151.0927 | 24.290 |
| 12.3 | 1.720 | 2.2756 | 0.593 | 0.676 | 19.5626 | 3.1545 | 104.713 | 15.958 |
| 14.3 | 1.650 | 2.2182 | 0.516 | 0.469 | 16.6151 | 2.673 | 79.639 | 12.358 |
| 16.3 | 1.650 | 2.1608 | 0.439 | 0.359 | 14.2379 | 2.320 | 60.083 | 10.361 |
| 18.3 | 1.650 | 2.1034 | 0.362 | 0.256 | 11.7275 | 1.949 | 52.548 | 8.401 |
| 20.3 | 1.650 | 2.0460 | 0.337 | 0.182 | 10.2690 | 1.723 | 46.903 | 7.614 |
| 22.3 | 1.650 | 1.9886 | 0.311 | 0.140 | 8.9609 | 1.520 | 42.021 | 6.934 |
| 24.3 | 1.650 | 1.9312 | 0.286 | 0.126 | 7.6557 | 1.313 | 38.041 | 6.358 |
| 26.3 | 1.650 | 1.8738 | 0.286 | 0.126 | 7.2890 | 1.249 | 38.014 | 6.349 |
| 28.3 | 1.650 | 1.8164 | 0.286 | 0.126 | 6.7715 | 1.159 | 37.975 | 6.336 |
| 30.3 | 1.650 | 1.7590 | 0.286 | 0.126 | 6.2735 | 1.072 | 37.935 | 6.332 |
| 32.3 | 1.650 | 1.7017 | 0.286 | 0.126 | 5.7959 | 0.989 | 37.896 | 6.309 |
| 34.3 | 1.650 | 1.6443 | 0.286 | 0.126 | 5.3369 | 0.909 | 37.857 | 6.296 |
| 36.3 | 1.650 | 1.5869 | 0.286 | 0.126 | 4.8974 | 0.833 | 37.818 | 6.282 |
| 38.3 | 1.650 | 1.5295 | 0.286 | 0.126 | 4.4774 | 0.761 | 37.778 | 6.269 |
| 40.8 | 1.650 | 1.4577 | 0.286 | 0.126 | 3.9793 | 0.675 | 37.729 | 6.252 |
| 42.3 | 1.740 | 1.6647 | 0.304 | 0.126 | 5.979 | 1.009 | 43.986 | 7.241 |
| 44.3 | 1.920 | 1.6970 | 0.410 | 0.126 | 7.7065 | 1.362 | 71.2332 | 11.276 |
| 46.3 | 2.150 | 1.8500 | 0.575 | 2.150 | 12.8540 | 2.269 | 135.6900 | 28.659 |

| R, in. | $EI_{co} \times 10^6$, lb/in.$^2$ | EA, $10^{-6}$, lb | A, in.$^2$ | GK $10^6$, lb/in.$^2$ | Wt/in., lb/in. | $I_\theta$, $lb_m \cdot in.^2/in.$ | Neutral axis separation, in. | $EC_w$ $10^6$, lb/in.$^4$ |
|---|---|---|---|---|---|---|---|---|
| 4.5 | 45.135 | 64.253 | 9.830 | 29.560 | 0.688 | 4.224 | 3.600 | 419.78 |
| 5.3 | 36.241 | 81.147 | 19.408 | 26.215 | 1.359 | 6.632 | 3.550 | 404.43 |
| 6.3 | 31.728 | 76.810 | 17.627 | 15.747 | 1.233 | 5.746 | 3.488 | 157.90 |
| 8.3 | 13.087 | 61.355 | 12.338 | 6.425 | 0.864 | 3.553 | 3.499 | 65.85 |
| 10.3 | 6.908 | 43.929 | 7.983 | 1.627 | 0.559 | 2.077 | 3.378 | 25.68 |
| 12.3 | 3.905 | 33.485 | 5.554 | 0.52145 | 0.389 | 1.338 | 3.289 | 11.94 |
| 14.3 | 3.197 | 27.440 | 4.518 | 0.3096 | 0.316 | 1.052 | 3.224 | 7.73 |
| 16.3 | 2.767 | 22.657 | 3.818 | 0.1936 | 0.267 | 0.888 | 3.221 | 5.75 |
| 18.3 | 2.235 | 17.716 | 3.095 | 0.1134 | 0.217 | 0.725 | 3.245 | 4.18 |
| 20.3 | 1.885 | 15.228 | 2.724 | 0.0931 | 0.191 | 0.654 | 3.328 | 3.28 |
| 22.3 | 1.587 | 13.307 | 2.435 | 0.0756 | 0.170 | 0.592 | 3.391 | 2.73 |
| 24.3 | 1.399 | 11.944 | 2.226 | 0.0611 | 0.156 | 0.537 | 3.414 | 2.40 |
| 26.3 | 1.394 | 11.926 | 2.216 | 0.0610 | 0.155 | 0.532 | 3.416 | 2.26 |
| 28.3 | 1.387 | 11.900 | 2.201 | 0.0609 | 0.154 | 0.525 | 3.419 | 2.12 |
| 30.3 | 1.379 | 11.874 | 2.187 | 0.0607 | 0.153 | 0.518 | 3.423 | 1.98 |
| 32.3 | 1.372 | 11.847 | 2.172 | 0.0606 | 0.152 | 0.511 | 3.426 | 1.85 |
| 34.3 | 1.364 | 11.821 | 2.158 | 0.0605 | 0.151 | 0.504 | 3.429 | 1.72 |
| 36.3 | 1.357 | 11.795 | 2.143 | 0.0603 | 0.150 | 0.498 | 3.433 | 1.60 |
| 38.3 | 1.349 | 11.768 | 2.129 | 0.0602 | 0.149 | 0.492 | 3.436 | 1.48 |
| 40.8 | 1.340 | 11.735 | 2.111 | 0.0601 | 0.148 | 0.485 | 3.440 | 1.34 |
| 42.3 | 1.638 | 13.127 | 2.358 | 0.0734 | 0.165 | 0.578 | 3.504 | 1.91 |
| 44.3 | 2.8528 | 18.456 | 3.370 | 0.1673 | 0.236 | 0.885 | 3.656 | 2.47 |
| 46.3 | 8.2719 | 31.577 | 7.955 | 9.7500 | 0.557 | 2.165 | 3.681 | 45.34 |

Table 3 C-45 Inputs for BMR on BO 105

| Symbol | Definition | Value | Units |
|---|---|---|---|
| $M_f$ | Fuselage mass | 9.79 | lb-sec$^2$/in. |
| $I_{Fx}$ | Fuselage roll inertia | 4218.0 | lb-sec$^2$/in. |
| $I_{Fy}$ | Fuselage pitch inertia | 11790.0 | lb-sec$^2$/in. |
| $I_{Fxy}$ | Fuselage product of inertia | 0 | lb-sec$^2$/in. |
| $M_p$ | Pylon mass | 0 | lb-sec$^2$/in. |
| $I_{px}$ | Pylon roll inertia | 343.5 | lb-sec$^2$/in. |
| $I_{py}$ | Pylon pitch inertia | 1218.5 | lb-sec$^2$/in. |
| $I_{pxy}$ | Pylon product of inertia | 0 | lb-sec$^2$/in. |
| $M_t$ | Tail boom mass | 0.2854 | lb-sec$^2$/in. |
| $I_{Tx}$ | Tail-boom roll inertia | 1040.0 | lb-sec$^2$/in. |
| $I_{Ty}$ | Tail-boom pitch inertia | 1735.0 | lb-sec$^2$/in. |
| $I_{Tz}$ | Tail-boom yaw inertia | 2775.0 | lb-sec$^2$/in. |
| $I_{Txy}$ | Tail-boom product of inertia | 0 | lb-sec$^2$/in. |
| $I_{Txz}$ | Tail-boom product of inertia | 0 | lb-sec$^2$/in. |
| $I_{Tyz}$ | Tail-boom product of inertia | 0 | lb-sec$^2$/in. |
| $e_o$ | Hub offset | 0 | in. |
| $e_1$ | Distance from hub center to first hinge | 22.03 | in. |
| $e_2$ | Distance between first and second hinge | 2.92 | in. |
| $e_3$ | Distance between second and third hinge | 20.05 | in. |
| $l_f$ | Horizontal distance to $M_f$ | 14.57 | in. |
| $h_f$ | Vertical distance to $M_f$ | 7.28 | in. |
| $l_2$ | Horizontal distance from A/C Ref axis to rotor shaft | 0 | in. |
| $l_3$ | Horizontal distance from rotor shaft to tail hinge | 106.3 | in. |
| $h_3$ | Vertical distance from A/C Ref axis to pylon hinge | 19.68 | in. |
| $h_4$ | Vertical distance from pylon hinge to hub center | 41.77 | in. |
| $l_p$ | Horizontal distance from rotor shaft to $M_p$ | 0 | in. |
| $h_p$ | Vertical distance from pylon hinge to $M_p$ | 30.94 | in. |
| $l_t$ | Horizontal distance from tail hinge to $M_t$ | 110.24 | in. |
| $h_t$ | Vertical distance from tail hinge to $M_t$ | 23.61 | in. |
| $h_2$ | Vertical distance from A/C Ref axis to tail hinge | 11.81 | in. |
| $f_1$ | Lateral distance from A/C Ref to aft landing gears | 48.0 | in. |
| $f_2$ | Lateral distance from A/C Ref to fwd landing gears | 48.0 | in. |
| $h_o$ | Vertical distance from A/C Ref to fwd landing gears | 49.0 | in. |
| $h_1$ | Vertical distance from A/C Ref to aft landing gears | 49.0 | in. |
| $l_1$ | Horizontal distance from A/C Ref axis to fwd landing gears | 68.0 | in. |
| $l_3'$ | Horizontal distance from rotor shaft axis to aft landing gears | 33.0 | in. |
| R | Blade radius | 193.37 | in. |
| $e_a$ | Blade cutout from hub center | 52.0 | in. |
| $\theta_o$ | Nose-up pitch at hub center | 12.5 | deg |
| $\theta_1$ | Nose-up pitch before first hinge | -2.34 | deg |
| $\theta_2$ | Nose-up pitch before second hinge | -0.722 | deg |

Table 3 Concluded

| Symbol | Definition | Value | Units |
|---|---|---|---|
| $\theta_3$ | Nose-up pitch before third hinge | -5.0 | deg |
| $\beta_o$ | Tip-up flap at hub center | -0.069 | deg |
| $\beta_1$ | Tip-up flap before first hinge | -0.116 | deg |
| $\beta_2$ | Tip-up flap before second hinge | -0.302 | deg |
| $\beta_3$ | Tip-up flap before third hinge | 0.0213 | deg |
|  | blade Lock number | 6.44 |  |
| $I_a$ | Blade flapping inertia | 1516.0 | lb-sec$^2$/in. |
|  | rotor speed | 425.0 | rpm |
| N | Number of blades | 4 |  |
| $K_{H1}$ | Rotational spring around first hinge | 99092.0 | in./lb-rad |
| $K_{H2}$ | Rotational spring around second hinge | 690000.0 | in./lb-rad |
| $K_{H3}$ | Rotational spring around third hinge | 40970.0 | in./lb-rad |
| $K\Phi_x$ | Pylon roll spring | 12883000.0 | in./lb-rad |
| $K\Phi_y$ | Pylon pitch spring | 12833000.0 | in./lb-rad |
| $K\Phi_{ty}$ | Tail vertical spring | 5175900.0 | in./lb-rad |
| $K\Phi_{ty}$ | Tail lateral spring | 6563100.0 | in./lb-rad |
| $K_{x1}$ | Longitudinal spring rate of aft gear | 2218.0 | in./lb |
| $K_{x2}$ | Longitudinal spring rate of fwd gear | 2218.0 | in./lb |
| $K_{y1}$ | Lateral spring rate of aft gear | 4113.0 | in./lb |
| $K_{y2}$ | Lateral spring rate of fwd gear | 4113.0 | in./lb |
| $K_{z1}$ | Vertical spring rate of aft gear | 4113.0 | in./lb |
| $K_{z2}$ | Vertical spring rate of fwd gear | 4113.0 | in./lb |
| $\eta_{H1}$ | Viscous damping around first hinge | 0 | 1. = 100% |
| $\eta_{H2}$ | Viscous damping around second hinge | 0.01 | 1. = 100% |
| $\eta_{H3}$ | Viscous damping around third hinge | 0 | 1. = 100% |
| $\beta_4$ | Blade tip-up flap after third hinge | 1.68 | deg |

## Appendix B - Experimental Data

The experimental data tabulated in this appendix were obtained from Ref. 1. Table 4 provides the modal damping for Case 1 as a function of the collective pitch. This is the ground resonance condition with the original or unstiffened landing gear and corresponds to Fig. 41 (in part) of Ref. 1. Table 5 shows the modal damping as a function of collective pitch for Case 2, the ground resonance condition with the stiffened landing gear. These data also correspond to Fig. 41 of Ref. 1. The Case 3 data are shown in Table 6 where the modal damping data as a function of airspeed are given for 1-g flight. These data correspond to Fig. 48 of Ref. 1. The data for Case 4 correspond to Fig. 51 of Ref. 1 and are shown in Table 7. The modal data were obtained at a constant airspeed of 50 knots and the collective pitch was varied to change the rate of climb (or descent).

Table 4 Case 1 Regressing Lead-Lag Mode Damping

| Collective pitch, percent | $\zeta_r$, percent |
|---|---|
| 17 | 0.9 |
| 17 | 1.033 |
| 20 | 1.77 |
| 24 | 2.36 |
| 31 | 2.47 |
| 31 | 2.48 |
| 38 | 3.26 |

Table 5 Case 2 Lead-Lag Regressing Mode Damping

| Collective pitch, percent | $\zeta_r$, percent |
|---|---|
| 0 | 1.49 |
| 10 | 1.94 |
| 17 | 2.22 |
| 23 | 2.59 |
| 26 | 2.32 |
| 26 | 2.58 |
| 29 | 1.49 |
| 32 | 1.38 |
| 32 | 1.62 |
| 35 | 1.70 |
| 35 | 1.97 |
| 43 | 3.68 |
| 50 | 4.07 |

Table 6 Case 3 Regressing Lead-Lag Mode Damping

| $V_{indicated}$, knots | $\zeta_r$, percent |
|---|---|
| 0 | 6.03 |
| 20 | 3.68 |
| 20 | 3.73 |
| 40 | 3.08 |
| 50 | 3.48 |
| 50 | 3.30 |
| 60 | 3.96 |
| 60 | 3.77 |
| 70 | 3.95 |
| 70 | 4.27 |
| 80 | 4.22 |
| 80 | 5.46 |
| 80 | 4.39 |
| 80 | 4.12 |
| 90 | 5.55 |
| 90 | 6.23 |
| 100 | 6.28 |
| 100 | 5.07 |
| 106 | 5.21 |

Table 7 Case 4 Regressing Lead-Lag Mode Damping

| Collective pitch, percent | $\zeta_r$, percent |
|---|---|
| -1 | 2.00 |
| 5 | 1.62 |
| 6 | 0.97 |
| 8 | 1.09 |
| 11 | 1.42 |
| 11 | 1.89 |
| 14 | 1.37 |
| 16 | 1.27 |
| 17 | 2.02 |
| 20 | 1.44 |
| 23 | 1.75 |
| 25 | 2.12 |
| 28 | 1.82 |
| 29 | 2.20 |
| 32 | 2.14 |
| 35 | 2.45 |
| 37 | 3.30 |
| 41 | 3.30 |
| 41 | 3.48 |
| 43 | 1.77 |
| 48 | 3.59 |
| 54 | 4.96 |
| 55 | 3.95 |
| 58 | 4.35 |
| 60 | 3.96 |

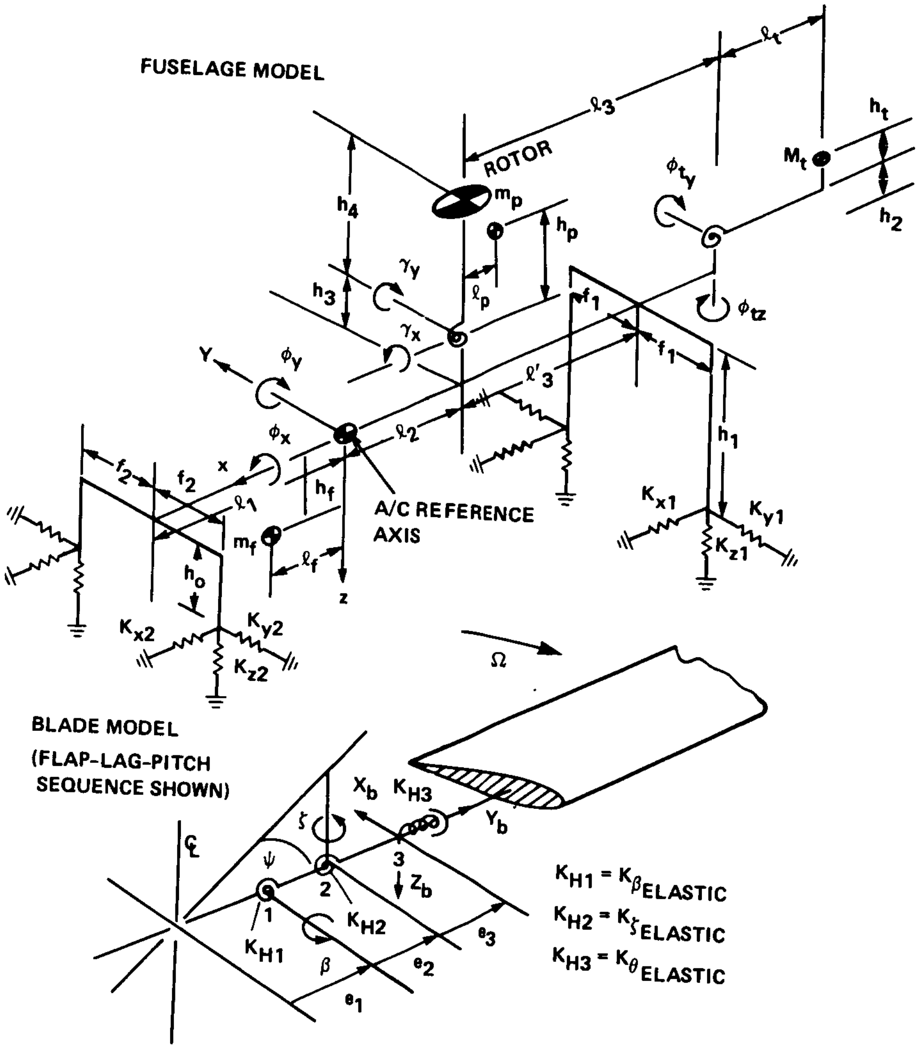

Fig. 10 Terms of reference for program C-45.

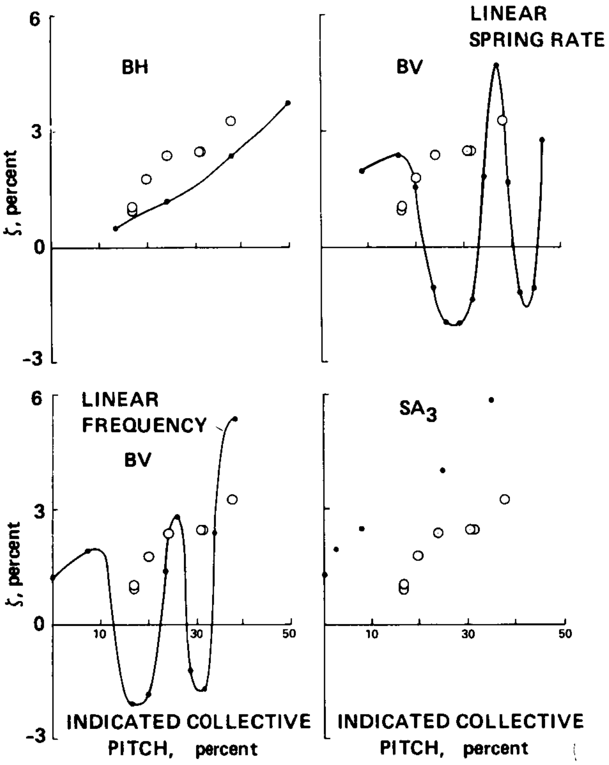

Fig. 11 Individual comparison for Case 1 modal damping as a function of collective pitch.

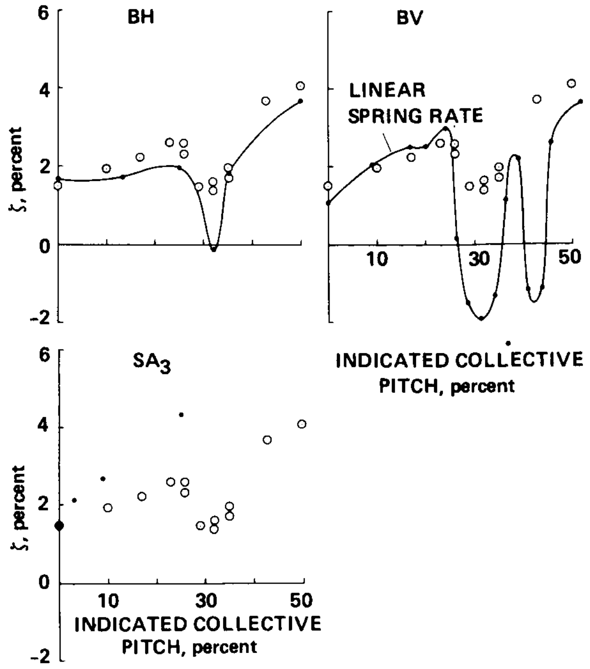

Fig. 13 Individual comparison for Case 2 modal damping as a function of collective pitch.

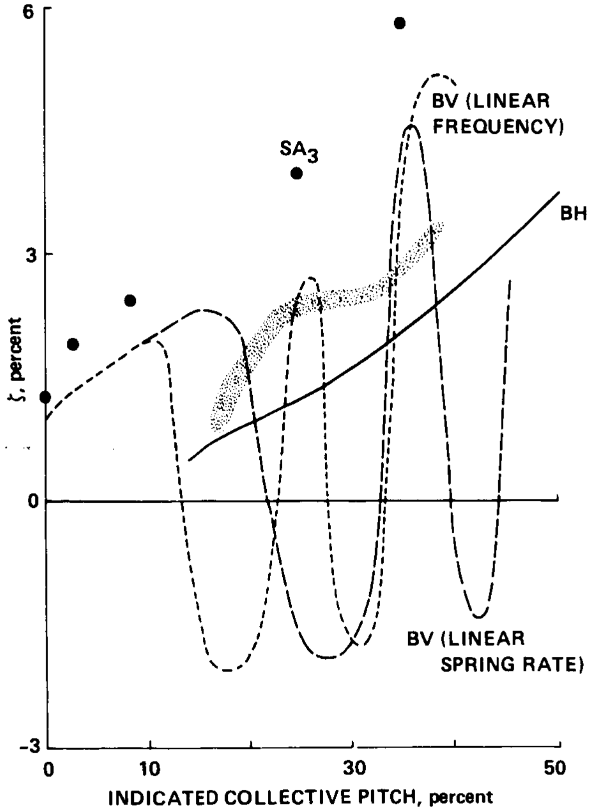

Fig. 12 Composite comparison for Case 1 modal damping as a function of collective pitch.

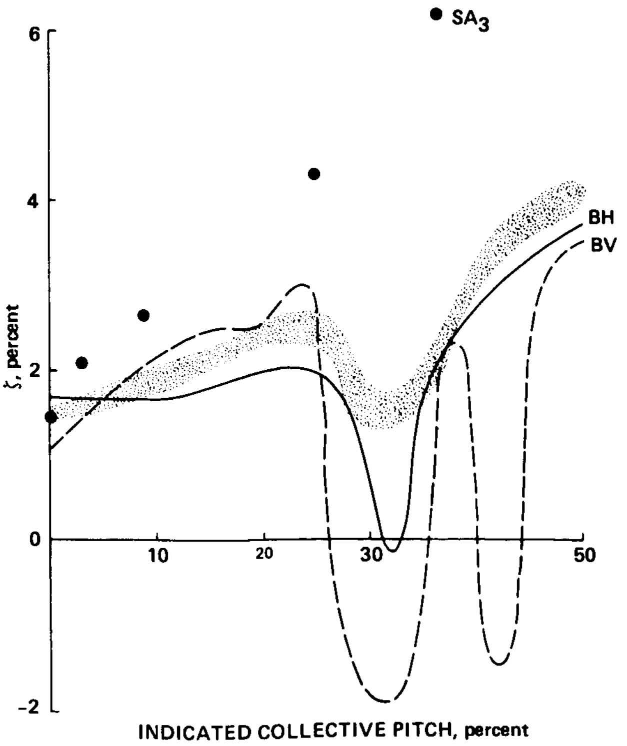

Fig. 14 Composite comparison for Case 2 modal damping as a function of collective pitch.

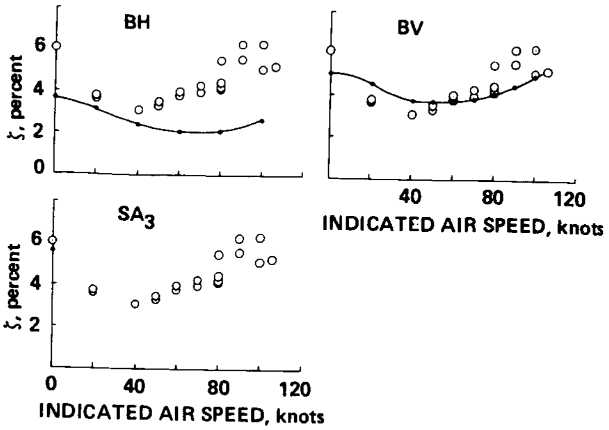

Fig. 15 Individual comparison for Case 3 modal damping as a function of indicated air speed.

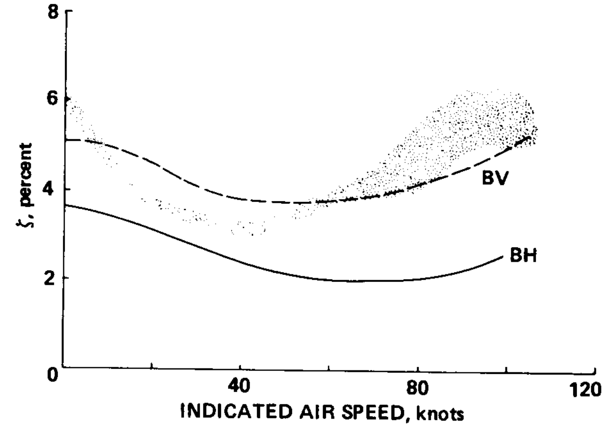

Fig. 16 Composite comparison for Case 3 modal damping as a function of indicated air speed.

## Appendix C - Correlation

All the theoretical predictions and experimental data are shown in this appendix. In some cases figures from the main text are repeated here for completeness. Two formats are used for the correlation. The first format compares the theoretical predictions and experimental data individually for each mathematical model used. In this format the actual calculated points are shown as solid symbols and the fairing between points was calculated by the experiment analysts and are shown as open symbols. The second format compares all the theoretical predictions on a single composite plot using the faired curve from the first format; the experimental data are shown as a stippled area. A code is used to identify the theoretical predictions for both the individual and composite comparisons and is explained in Table 8.

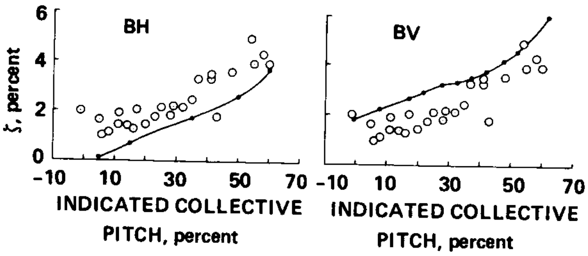

Fig. 17 Individual comparison for Case 4 modal damping as a function of collective pitch at 50 knots.

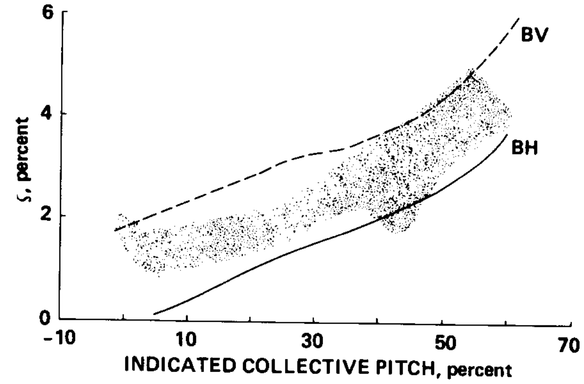

Fig. 18 Composite comparison for Case 4 modal damping as a function of collective pitch at 50 knots.

Table 8 Explanation of Prediction Codes

| ID | Prediction Method | User |
|---|---|---|
| BH | DRAV21 (hover)<br>C81 (forward flight) | Bell Helicopter Textron |
| BV | C-90 | Boeing Vertol |
| SA$_3$ | E927-3 | Sikorsky Aircraft |